

Constraints on neutrino oscillation parameters from the SNO salt phase data

Abhijit Bandyopadhyay¹, Sandhya Choubey^{2,3}, Srubabati Goswami^{4,5}, S.T. Petcov^{3,2,6}, D.P. Roy⁷

¹*Saha Institute of Nuclear Physics, 1/AF, Bidhannagar, Calcutta 700 064, India,*

²*INFN, Sezione di Trieste, Trieste, Italy,*

³*Scuola Internazionale Superiore di Studi Avanzati, I-34014, Trieste, Italy,*

⁴*Harish-Chandra Research Institute, Chhatnag Road, Jhusi, Allahabad 211 019, India,*

⁵*The Abdus Salam International Centre for Theoretical Physics, I-34100, Trieste, Italy,*

⁶*Institute of Nuclear Research and Nuclear Energy, Bulgarian Academi of Science, Sofia, Bulgaria,*

⁷*Tata Institute of Fundamental Research, Homi Bhabha Road, Mumbai 400 005, India*

Abstract

The physics implications of the just published salt phase data from the SNO experiment are examined. The effect of these data on the allowed ranges of the solar neutrino oscillation parameters, Δm_{21}^2 and $\sin^2 \theta_{12}$, are studied in the cases of two- and three- neutrino mixing. In the latter case we derive an upper limit on the angle θ_{13} . Constraints on the solar ν_e transitions into a mixture of active and sterile neutrinos are also presented. Finally, we give predictions for the day-night asymmetry in the SNO experiment, for the event rate in the BOREXINO and LowNu experiments, and discuss briefly the constraints on the solar neutrino oscillation parameters which can be obtained with prospective KamLAND data.

1 Introduction

The past two years have witnessed remarkable experimental progress in the studies of neutrino mixing and oscillations. The latest addition to this magnificent effort is the salt phase data from the SNO experiment [1].

In 2001, the evidences for solar neutrino oscillations [2] obtained in the pioneer experiment of Davis et al. (Homestake) [3, 4], and in the Kamiokande, SAGE, GALLEX/GNO [5] and Super-Kamiokande [6] experiments, were reinforced by the first results of the SNO experiment on the charged current (CC) reaction on deuterium induced by solar neutrinos [7]. In conjunction with the Super-Kamiokande (SK) $\nu - e^-$ scattering data, the SNO CC data established the existence of solar ν_e flavour conversion with a statistical significance of 3.3 s.d.. This conclusion was further corroborated by the 2002 SNO data on the neutral current (NC) reaction on deuterium, caused by solar neutrinos [8]. The combined CC and NC SNO data showed the presence at 5.3 s.d. of a nonzero $\nu_{\mu,\tau}$ and/or $\bar{\nu}_{\mu,\tau}$ component in the flux of the solar 8B neutrinos reaching the Earth. At each stage, the SNO data enabled one to determine with improved precision the average solar ν_e survival probability P_{ee} from the CC reaction data, and the 8B flux normalisation f_B from the data on the NC reaction. This in turn led to a diminishing of the allowed regions of values of the two parameters - the neutrino mass squared difference Δm_{21}^2 ($\equiv \Delta m_{\odot}^2$) and the mixing angle θ_{12} ($\equiv \theta_{\odot}$), characterizing the solar neutrino oscillations. The SNO CC data had the main impact of ruling out the Small Mixing Angle (SMA) MSW [9] region in conjunction with the SK data [7, 10]. The SNO data from the D_2O phase¹ clearly showed preference for the Large Mixing Angle (LMA) MSW solution of the solar neutrino problem, disfavoring the relatively low Δm_{21}^2 (LOW, QVO) solutions [8, 11]. The first results of the KamLAND experiment [12], under the plausible assumption of CPT-invariance in the lepton sector, established the LMA solution as unique solution of the solar neutrino problem.

The combined two-neutrino oscillation analyses of the solar neutrino and KamLAND data, available before the publication of the SNO salt phase results, identified two distinct solution sub-regions within the LMA solution region (see, e.g., [13, 14]). For the best fit values of Δm_{\odot}^2 and θ_{\odot} in the two sub-regions - low-LMA and high-LMA, it was found in [13], respectively: $\Delta m_{\odot}^2 = 7.2 \times 10^{-5} \text{ eV}^2$, $\sin^2 \theta_{\odot} = 0.3$, and $\Delta m_{\odot}^2 = 1.5 \times 10^{-4} \text{ eV}^2$, $\sin^2 \theta_{\odot} = 0.3$. The low-LMA solution was preferred statistically by the data. At 99.73% C.L. one obtained [13]:

$$\Delta m_{\odot}^2 \cong (5.0 - 20.0) \times 10^{-5} \text{ eV}^2, \quad \sin^2 \theta_{\odot} \cong (0.21 - 0.47). \quad (1)$$

In the case of 3-neutrino mixing, the analysis of the solar neutrino and KamLAND data involves an additional parameter θ_{13} - the neutrino mixing angle limited by the CHOOZ and Palo Verde experiments [15]. The precise upper limit on $\sin^2 \theta_{13}$ depends on the value of Δm_{31}^2 - the neutrino mass squared difference responsible for the atmospheric ν_{μ} and $\bar{\nu}_{\mu}$ oscillations (see, e.g., [16]). The preliminary results of an improved analysis of the SK atmospheric neutrino data, performed recently by the SK collaboration, gave [17]

$$1.3 \times 10^{-3} \text{ eV}^2 \lesssim \Delta m_{31}^2 \lesssim 3.1 \times 10^{-3} \text{ eV}^2, \quad 90\% \text{ C.L.}, \quad (2)$$

¹Here, and in the rest of the the paper, by D_2O phase we mean the NC reactions due to the final state neutron capture on deuterium.

Data set used	best-fit parameters		99% C.L. allowed range	
	$\Delta m_{21}^2 / (10^{-5} \text{eV}^2)$	$\sin^2 \theta_{12}$	$\Delta m_{21}^2 / (10^{-5} \text{eV}^2)$	$\sin^2 \theta_{12}$
Cl+Ga+SK+ D_2O	6.06	0.29	3.2 – 24.5	0.21 – 0.44
Cl+Ga+SK+salt	6.08	0.28	3.0 – 23.7	0.19 – 0.43
Cl+Ga+SK+ D_2O +salt	6.06	0.29	3.2 – 17.2	0.22 – 0.40
Cl+Ga+SK+ D_2O +KL	7.17	0.3	5.3 – 9.9	0.22 – 0.44
Cl+Ga+SK+ D_2O +salt+KL	7.17	0.3	5.3 – 9.8	0.22 – 0.40

Table 1: The best-fit values of the solar neutrino oscillation parameters, obtained using different combinations of data sets. Shown also are the 99% C.L. (corresponding to $\Delta\chi^2$ for a 2 parameter fit) allowed ranges of the parameters from the different analyses.

with a best fit value $\Delta m_{31}^2 = 2.0 \times 10^{-3} \text{ eV}^2$.

After the KamLAND results the two major issues to be settled with the future solar neutrino and KamLAND data are:

- Resolving the ambiguity between the low-LMA and the high-LMA solutions and thereby obtaining tighter constraints on Δm_{21}^2 .
- Constraining further the allowed range of the solar neutrino mixing angle, θ_{12} .

In the present article we examine some of the physics implications of the latest salt phase data from SNO [1]. We study, in particular, the effect of these data on the allowed ranges of the solar neutrino oscillation parameters, Δm_{21}^2 and $\sin^2 \theta_{12}$. This is done in the cases of two- and three-neutrino mixing. In the latter case we derive an upper limit on the angle θ_{13} . Constraints on the solar ν_e transitions into a mixture of active and sterile neutrinos, i.e., on the allowed sterile fraction, are also presented. Finally, we give predictions for the day-night asymmetry in the SNO experiment, for the event rate in the BOREXINO and LowNu experiments, and discuss briefly the constraints on the solar neutrino oscillation parameters which can be obtained with future KamLAND data.

2 Two-neutrino oscillation analysis

2.1 Analysis with global solar neutrino data

In this Section we first perform a two-neutrino oscillation analysis of the global solar data, incorporating the new SNO results. We include the total rates from the radiochemical experiments Cl and Ga (Gallex, SAGE and GNO combined) [5] and the 1496 day 44 bin SK Zenith angle spectrum data [6]². For SNO we take the combined CC, NC and Electron Scattering (ES) 34 bin energy spectrum data from the D_2O phase [8], and the recently reported CC, NC and ES rates

²SK has recently reanalyzed their day/night data with improved precision [18]. However, the information content in [18] is not enough for including it in our analysis.

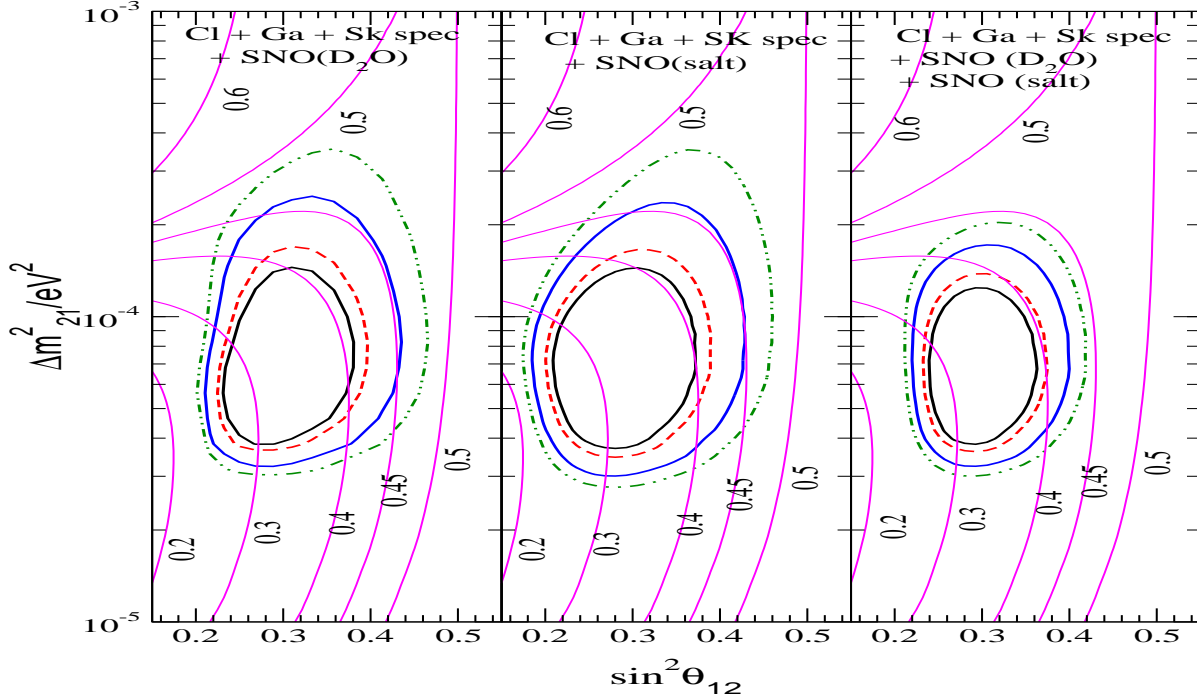


Figure 1: The 90%, 95%, 99% and 99.73% C.L. allowed regions in the $\Delta m_{21}^2 - \sin^2 \theta_{12}$ plane from global χ^2 -analysis of the data from solar neutrino experiments. We use $\Delta\chi^2$ values to plot the C.L. contours corresponding to a two parameter fit. Also shown are the lines of constant CC/NC event rate ratio $R_{CC/NC}$.

from the latest salt phase of the experiment [1]³. To ascertain the impact of the salt phase data and facilitate comparison between the impact of the data from the different phases, we include the SNO data in the following three ways in our analysis.

1. Use only the CC+ES+NC day/night spectra data from the D_2O phase,
2. Use only the CC, ES and NC event rate data from the salt phase,
3. Use data from both phases together.

We follow the instructions given in [19] by the SNO Collaboration to treat the SNO data.

³Note that the salt enriched data from SNO gives the CC, ES and NC total rates without any assumption on the 8B spectrum shape.

For our statistical analysis of the global solar neutrino data we follow a covariant approach and minimise the χ^2 defined as

$$\chi_{\odot}^2 = \sum_{i,j=1}^N (R_i^{\text{expt}} - R_i^{\text{theory}})(\sigma_{ij}^2)^{-1}(R_j^{\text{expt}} - R_j^{\text{theory}}) \quad (3)$$

where R_i are the solar data points, N is the number of data points and $(\sigma_{ij}^2)^{-1}$ is the inverse of the covariance matrix, containing the squares of the correlated and uncorrelated experimental and theoretical errors. We leave the 8B flux normalisation factor f_B to vary freely in our analysis. For further details of our solar neutrino data analysis we refer the reader to [10, 11].

The results of the analysis of the global solar neutrino data are presented in Table 1 and Figure 1. Table 1 gives the best-fit points and the allowed range of parameter values. The best-fit for the global analysis, including the complete SNO data from both phases, is obtained at $\Delta m_{21}^2 = 6.06 \times 10^{-5} \text{ eV}^2$, $\sin^2 \theta_{12} = 0.29$ and $f_B = 1.04$. Note that if we consider only the salt phase data from SNO, the best-fit value of $\sin^2 \theta_{12}$ is marginally lower.

In the first panel of Figure 1 we show the allowed region in the parameter space when only the spectrum data from the D_2O phase is included. In the second panel we show the allowed areas including the SNO salt phase data but excluding the SNO spectrum data from the D_2O phase. A comparison of the first two panels shows that with the exclusion of the D_2O phase spectrum data, the allowed region enlarges in size. Even though the SNO data from the D_2O phase agrees remarkably well with the salt phase data, the ratio of CC and NC event rates, $R_{CC/NC}$, is slightly different for the two phases. In particular, for the D_2O phase, if one uses the data given by SNO for the null hypothesis, one gets for the ratio $R_{CC/NC} = 0.346$. For the salt phase, the ratio is $R_{CC/NC} = 0.306$. Thus, the CC to NC event rate ratio has decreased, which has very important implications [20]. In Figure 1 we have superimposed the iso- $R_{CC/NC}$ contour lines (see [20]) on the allowed regions in the $\Delta m_{21}^2 - \sin^2 \theta_{12}$ plane. The figure clearly shows that since the $R_{CC/NC}$ for the salt phase data is lower, the allowed regions shift left, following the iso- $R_{CC/NC}$ contours. This results in the shift of the allowed range of $\sin^2 \theta_{12}$ to smaller values (see Table 1). The allowed Δm_{21}^2 shift to lower values as well for the same reason.

The third panel shows the allowed regions, obtained by including the SNO data from both the D_2O phase and the salt phase. Following the SNO collaboration [19], we treat these two phases as separate experiments with no correlation between them. Combination of the salt phase and the D_2O phase data produce a more restrictive upper bound on $\Delta m_{21}^2 \leq 1.7 \times 10^{-4} \text{ eV}^2$ (99.73% C.L.). The upper limit on $\sin^2 \theta_{12}$ also improves compared to what we have before the salt phase data, as can be seen by comparing the first panel with the last one in Figure 1. The exact intervals in which the solar neutrino oscillations parameters are constrained to lie are given in Table 1.

2.2 Constraints from combined solar and KamLAND data

We next include the 162 ton-year results from the KamLAND experiment into the analysis. We use the 13 bin KamLAND spectrum data and defined a χ^2 assuming a Poissonian distribution as

$$\chi_{klspec}^2 = \sum_i \left[2(X_n S_{KL,i}^{\text{theory}} - S_{KL,i}^{\text{expt}}) + 2S_{KL,i}^{\text{expt}} \ln\left(\frac{S_{KL,i}^{\text{expt}}}{X_n S_{KL,i}^{\text{theory}}}\right) \right] + \frac{(X_n - 1)^2}{\sigma_{sys}^2} \quad (4)$$

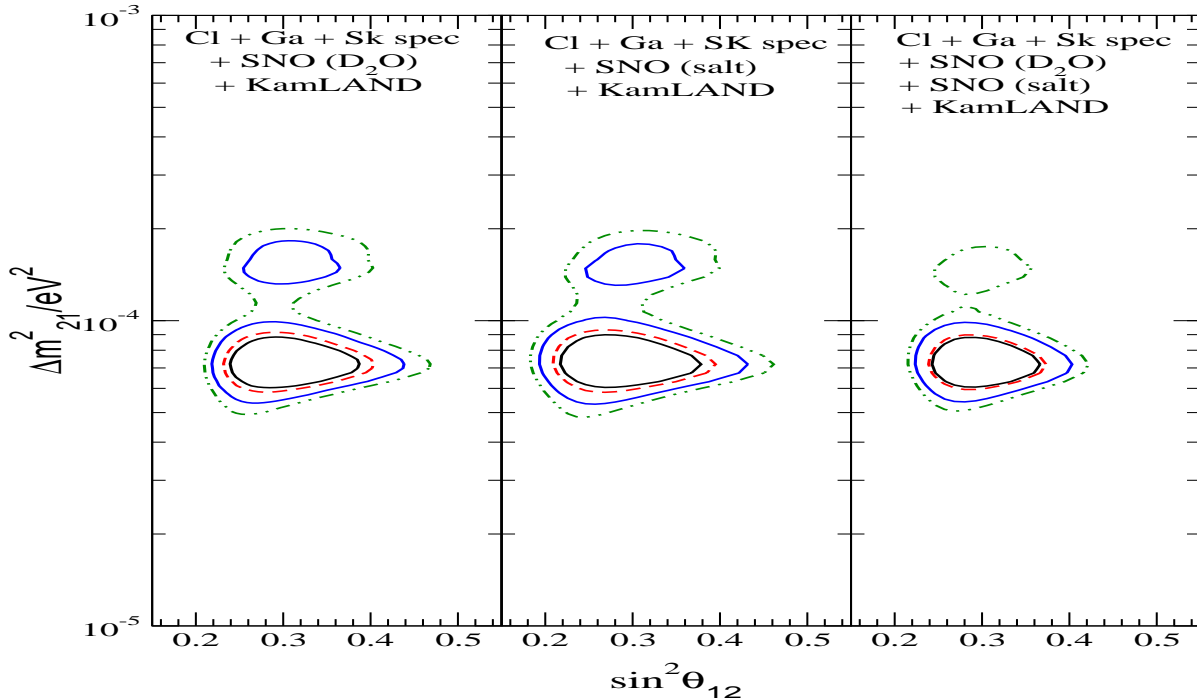


Figure 2: The 90%, 95%, 99% and 99.73% C.L. allowed regions in the $\Delta m_{21}^2 - \sin^2 \theta_{12}$ plane from global χ^2 -analysis of solar and KamLAND data. We use the $\Delta\chi^2$ values corresponding to a 2 parameter fit to plot the C.L. contours.

where σ_{sys} is taken to be 6.42% and X_n allowed to vary freely (see [13] for the details of the analysis). In the last 2 rows of Table 1 we give the best-fit data points and the allowed ranges of the parameters obtained before and after including the latest salt phase SNO data in the global analysis. The best-fit point for the combined global analysis is in the low-LMA region at $\Delta m_{21}^2 = 7.17 \times 10^{-5} \text{ eV}^2$ and $\sin^2 \theta_{12} = 0.30$. Thus, the best-fit values of the parameters for the combined solar+KamLAND data analysis do not change after inclusion of the latest SNO results. The best-fit $f_B = 1.02$.

In Figure 2 we present the corresponding allowed regions. Again we show results separately for only the D_2O phase (left-hand panel), only the salt phase (middle panel) and the global data, with the two phases combined (right-hand panel). Note the shift of the allowed regions in the middle panel which includes only the salt phase data, to smaller values of $\sin^2 \theta_{12}$. We find that although the separate inclusion of the data from each phase allows the high-LMA region at 99%

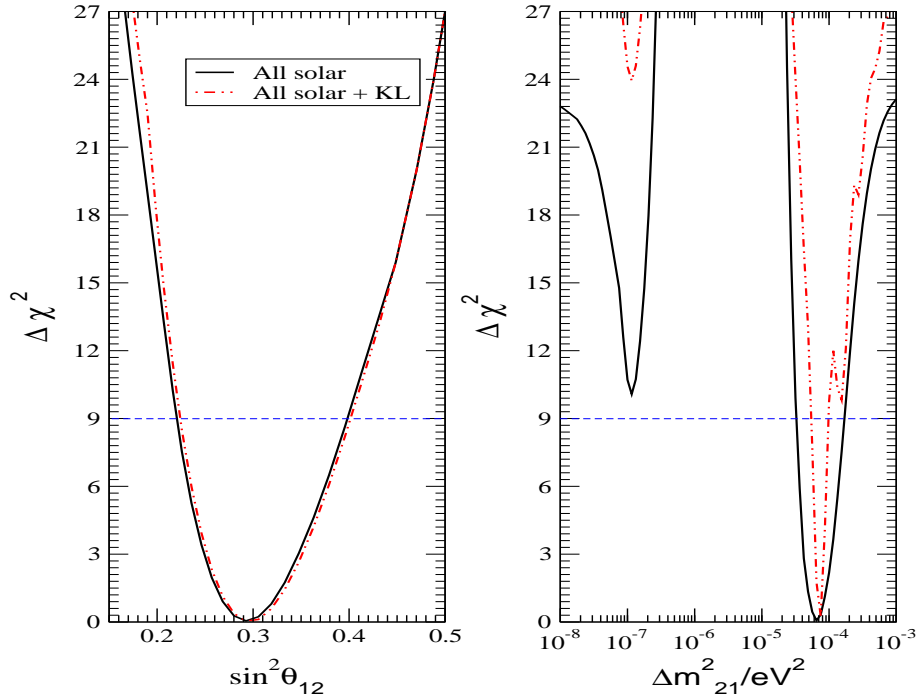


Figure 3: Bounds on Δm_{21}^2 and $\sin^2 \theta_{12}$ from the $\Delta\chi^2$ as a function of Δm_{21}^2 and $\sin^2 \theta_{12}$, respectively. The results shown in both panels are obtained by allowing all the other parameters to vary freely. The dashed line shows the 3σ limit corresponding to 1 parameter fit.

C.L., the combination of both allows the high-LMA region only at 3σ .

In Figure 3 we show the dependence of $\Delta\chi^2 = \chi^2 - \chi_{min}^2$ on Δm_{21}^2 (right-hand panel) and $\sin^2 \theta_{12}$ (left-hand panel), respectively, after marginalising over the remaining free parameters. The solid lines represent the $\Delta\chi^2$ for the global solar neutrino data, while the dashed curves correspond to the combined solar and KamLAND data. We note that the Δm_{21}^2 corresponding to the LOW solution is ruled out at slightly more than 3σ by the solar neutrino data alone, and at nearly 5σ from the combined solar and KamLAND data. KamLAND results are seen to produce a remarkable constraint on Δm_{21}^2 . Maximal mixing is now ruled out at more the 5σ level by the solar data alone. The KamLAND data does not put a strong constraint on $\sin^2 \theta_{12}$.

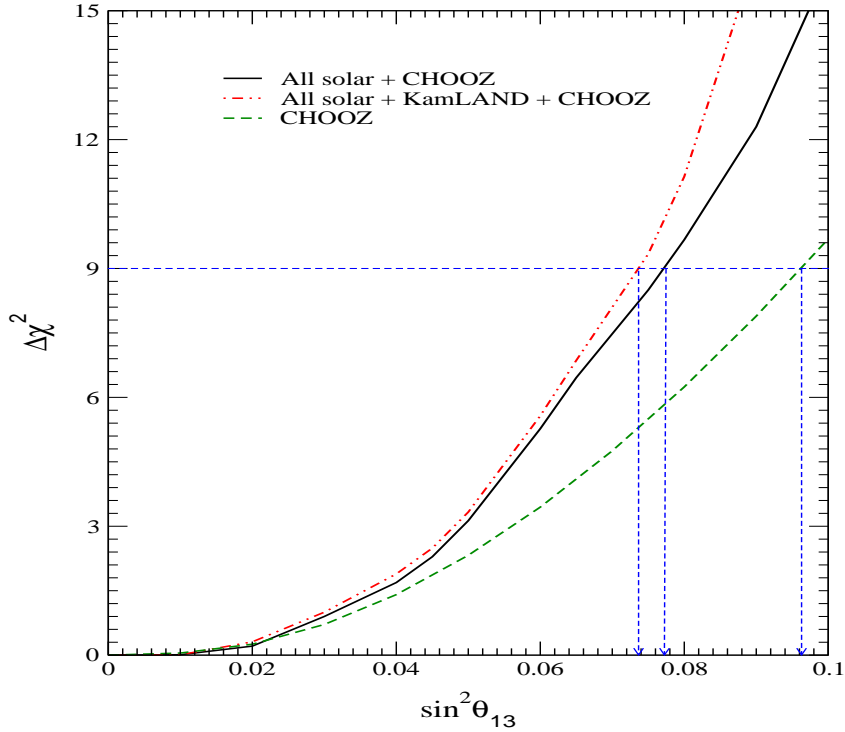


Figure 4: Bounds on the mixing angle θ_{13} from the global solar neutrino and CHOOZ data (solid line), and the combined solar, CHOOZ and KamLAND data (dashed line). All the other parameters are allowed to vary freely. The dashed line shows the 3σ limit corresponding to the case of 1 parameter fit.

3 Bounds from three-neutrino oscillation analysis

So far we have presented results obtained in the framework of two-neutrino oscillations, where the solar ν_e oscillates into another active neutrino with a different flavor. However, if the mixing angle θ_{13} which is restricted by the CHOOZ and Palo Verde data, is not zero, the solar ν_e oscillations will involve also the third heaviest neutrino mass eigenstate, with the associated neutrino mass squared difference given by Δm_{31}^2 . The relevant electron neutrino/antineutrino survival probability in the three-neutrino mixing case is given by the following expression:

$$P_{ee}^{3gen} = \cos^4 \theta_{13} P_{ee}^{2gen} + \sin^4 \theta_{13} \quad (5)$$

where P_{ee}^{2gen} is the ν_e survival probability for two-neutrino mixing (see, e.g., [21]). In the case of solar neutrinos, $P_{ee}^{2gen} \equiv P_{ee\odot}^{2gen}$ is the two-neutrino oscillation ν_e survival probability [22] with the so-

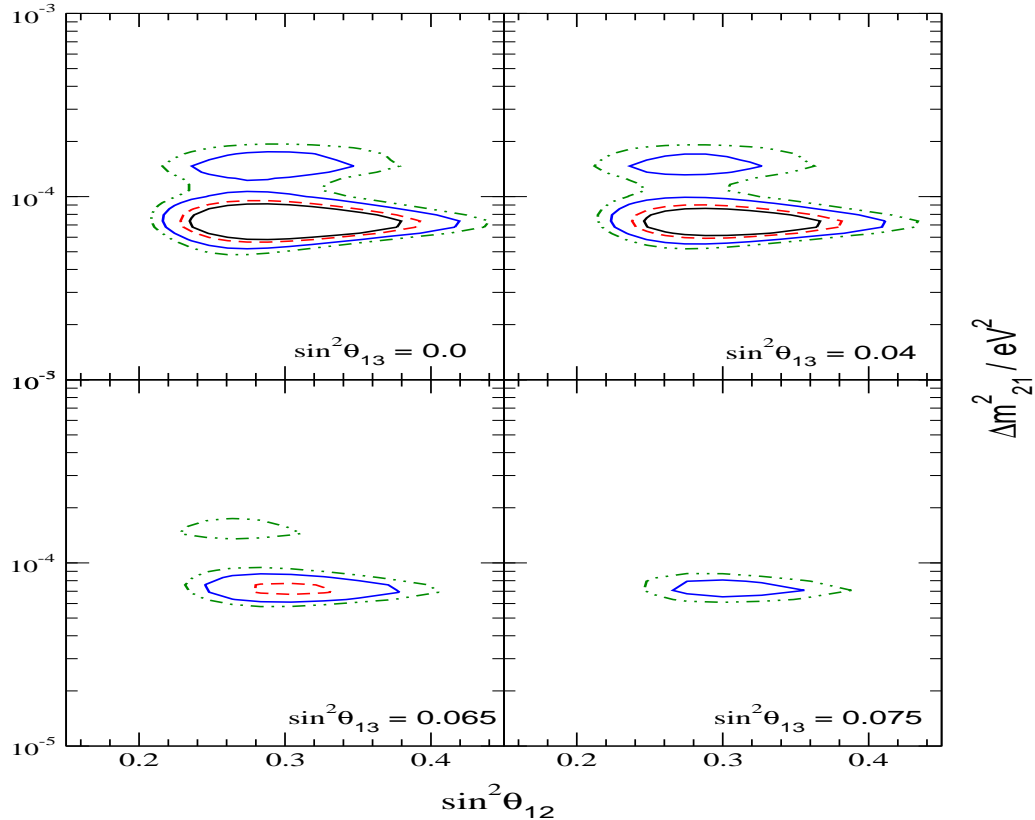


Figure 5: The 90%, 95%, 99% and 99.73% C.L. allowed contours in the $\Delta m_{21}^2 - \sin^2 \theta_{12}$ plane, from the three-neutrino oscillation analysis of the global solar and reactor data, including the data from the KamLAND and CHOOZ experiments. The different panels are drawn at different fixed values of $\sin^2 \theta_{13}$. Here we use three parameter fit $\Delta\chi^2$ values to plot the C.L. contours.

lar electron number density N_e replaced by $N_e \cos^2 \theta_{13}$. The term $\sin^4 \theta_{13}$ can to a good approximation be neglected in eq. (5). Since for the solar neutrinos one has $P_{ee\odot}^{2gen} \approx \sin^2 \theta_{12}$ in the low-LMA region, we have $P_{ee\odot}^{3gen} \approx \cos^4 \theta_{13} \sin^2 \theta_{12}$. For the reactor $\bar{\nu}_e$ detected in the KamLAND experiment, the matter effects are negligible and one gets $P_{eeKL}^{3gen} = \cos^4 \theta_{13} \{1 - \sin^2 2\theta_{12} \sin^2(\Delta m_{21}^2 L/4E)\}$, where L is the source-detector distance and E the antineutrino energy. From Eq. (5), we note that the presence of a non-zero θ_{13} shifts θ_{12} , obtained from the two-neutrino oscillation solar neutrino data analysis, to larger values. On the contrary, for the reactor antineutrinos, we should expect the allowed range of θ_{12} determined from a two-neutrino mixing analysis to shift to smaller values, if θ_{13} is non-zero and is sufficiently large. The survival probability for the short-baseline CHOOZ experiment is approximately given by $P_{eeCHOOZ}^{3gen} \approx 1 - \sin^2 2\theta_{13} \sin^2(\Delta m_{31}^2 L/4E)$ and is hence very sensitive to the range of allowed value of atmospheric neutrino mass squared difference, Δm_{31}^2 . We

use the 3σ allowed value of Δm_{31}^2 from the latest SK analysis of the atmospheric neutrino data [17]. We perform a combined three-neutrino oscillation analysis of the global solar neutrino and reactor data, including both the KamLAND and CHOOZ results.

In Figure 4 we present the $\Delta\chi^2$ obtained for various fixed values of $\sin^2\theta_{13}$, when all other parameters are allowed to vary freely. The 3σ bounds on $\sin^2\theta_{13}$, obtained from the global solar neutrino and CHOOZ data analysis, can be directly read from the figure as $\sin^2\theta_{13} < 0.077$. For the combined analysis with solar, CHOOZ and KamLAND data, the bound marginally tightens to $\sin^2\theta_{13} < 0.074$. We have checked that the bounds on Δm_{21}^2 and $\sin^2\theta_{12}$, even for the three-generation analysis, are the same as those given in Figure 3.

In Figure 5 we present the allowed regions in the $\Delta m_{21}^2 - \sin^2\theta_{12}$ plane, for four fixed values of θ_{13} . The presence of a small non-zero θ_{13} improves the fit in the regions of the parameter space with higher values of Δm_{21}^2 , i.e., in the high-LMA zone, where the 8B neutrino transitions are not affected by matter effects over the entire energy spectrum, and which therefore give a larger value of the CC/NC event rate ratio [20]. The presence of the $\cos^4\theta_{13}$ factor in the survival probability acts as a normalisation which effectively reduces the CC event rate and hence makes the high-LMA region less disfavored by the data. Since matter effects in the Sun are relatively small for the high-LMA values of Δm_{21}^2 , the allowed regions in these zones appear at smaller values of θ_{12} , as discussed above. However, as θ_{13} increases, the allowed areas shrink and finally vanish for $\sin^2\theta_{13} > 0.075$. Note that we get allowed regions at $\sin^2\theta_{13} = 0.075$ even though from Figure 4 the 3σ range appears to be $\sin^2\theta_{13} < 0.074$: in Figure 5 we use a $\Delta\chi^2$ which corresponds to a three parameter fit.

4 Constraints on transitions into a state with a sterile neutrino component

As is well known, the explanation of the positive evidences of oscillations from the LSND [23] experiment and the solar and atmospheric neutrino oscillation data requires the existence of a fourth neutrino which has to be inert. A comparison of the SNO CC and NC data from the D_2O phase had already ruled out solar ν_e oscillations into pure sterile state at 5.3 s.d. [8]. The inclusion of the SNO salt phase data raises the degree of disfavour to 7.8σ level [1]. However, transitions to “mixed” states, where the final neutrino state is a mixture of active and sterile components, is still allowed by the data. We find the limits on the sterile fraction from the global data.

We consider a general case where the ν_e produced in the Sun transforms into a “mixed” state given by $\nu' = \sin\alpha \nu_{active} + \cos\alpha \nu_{sterile}$. Thus, $\sin^2\alpha (\cos^2\alpha)$ gives the fraction of the active (sterile) component in the resultant solar neutrino flux at Earth. In Figure 6 we present the plots of $\Delta\chi^2$ vs f_B (left-hand panel), and $\Delta\chi^2$ vs $\sin^2\alpha$ (right-hand panel), allowing the mass and mixing parameters to vary freely in the LMA region. The solid lines give the constraints from the solar data alone, while the dashed lines correspond to the combined solar and KamLAND data. The range of allowed values of f_B , determined from the global solar (solar+KamLAND) data analysis at 3σ is $0.87 - 1.2$ (1.16). The allowed value for the sterile fraction in the resultant solar neutrino flux at Earth is constrained to $1 - \sin^2\alpha < 0.6$ (0.52) at 3σ by the solar (solar+KamLAND) data. Before the SNO salt phase data was announced, the corresponding limit for the sterile fraction at 3σ from the combined solar+KamLAND data analysis was $1 - \sin^2\alpha < 0.54$. Thus, the SNO salt

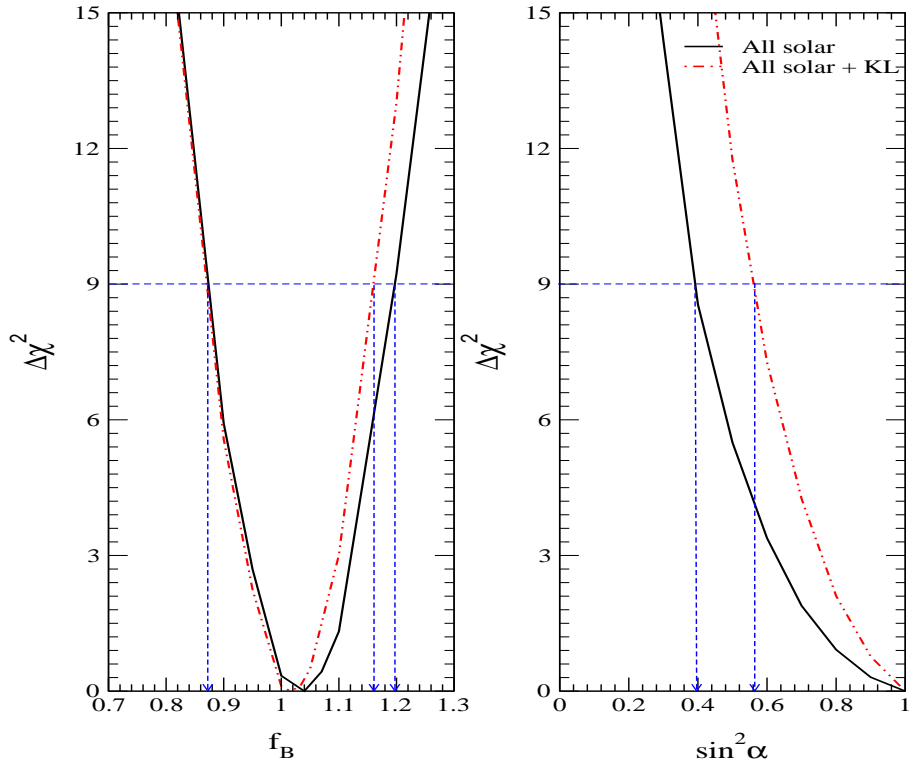


Figure 6: Bounds on f_B and the sterile fraction in the solar neutrino flux, given by $1 - \sin^2 \alpha$. The left panel shows the $\Delta\chi^2$ as a function of f_B , while the right-hand panel gives the corresponding bounds on $\sin^2 \alpha$. The $\Delta\chi^2$ is marginalised over all the oscillation parameters. The dashed line shows the 3σ limit corresponding to one parameter fit.

data is seen to only marginally tighten the noose on the possible presence of a sterile component in the solar neutrino flux.

5 Future and outlook

With the latest salt phase data from SNO giving further credence to the low-LMA solution, the stage is set for the precision era in the field of solar neutrino physics. The high-LMA solution stands disfavored and only a small area appears at 3σ level. The next phase of the SNO experiment will be devoted to obtaining neutral current data using Helium counters [24]. This would give a totally uncorrelated information on the CC and NC event rates observed at SNO. In the near future SNO is expected to provide data on the day/night spectrum, which could be used in a statistical analysis to further constrain the solar neutrino oscillation parameters [19]. One of the

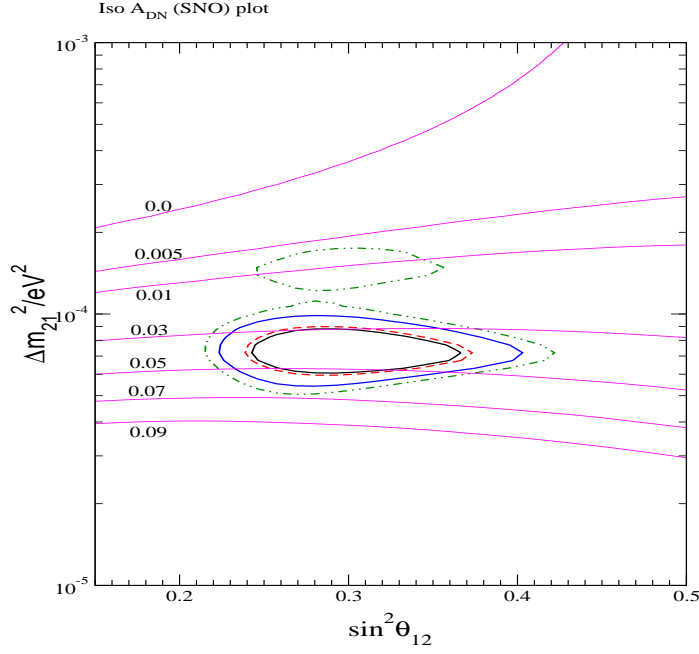


Figure 7: Lines of constant day-night asymmetry for the SNO experiment, superposed on the allowed region from the global analysis of the solar and KamLAND data.

related observables is the day-night asymmetry:

$$A_{DN} = 2 \frac{N - D}{N + D}. \quad (6)$$

The predicted A_{DN} in SNO, for the current best-fit values of the parameters in the low-LMA region, as well as the corresponding 3σ range, are given by (see also [20]):

$$A_{DN}^{SNO} = 0.04, \quad 3\sigma \text{ range : } 0.02 - 0.07, \quad \text{low - LMA}, \quad (7)$$

For the barely allowed high-LMA solution we get:

$$A_{DN}^{SNO} = 0.01, \quad 3\sigma \text{ range : } 0.007 - 0.02, \quad \text{high - LMA}. \quad (8)$$

In Figure 7 we show the lines of constant A_{DN} for SNO [20].

The potential of Borexino [25] and any generic electron scattering experiment for the low energy pp neutrinos – the LowNu experiments [26] – in constraining the mass and mixing parameters have been studied most recently in [27, 28]. The predicted rates for Borexino and LowNu experiments are

$$R_{Be} = 0.65, \quad (3\sigma \text{ range } \equiv 0.61 - 0.71); \quad \text{low - LMA} \quad (9)$$

$$R_{pp} = 0.71, \quad (3\sigma \text{ range } \equiv 0.67 - 0.76); \quad \text{low - LMA} \quad (10)$$

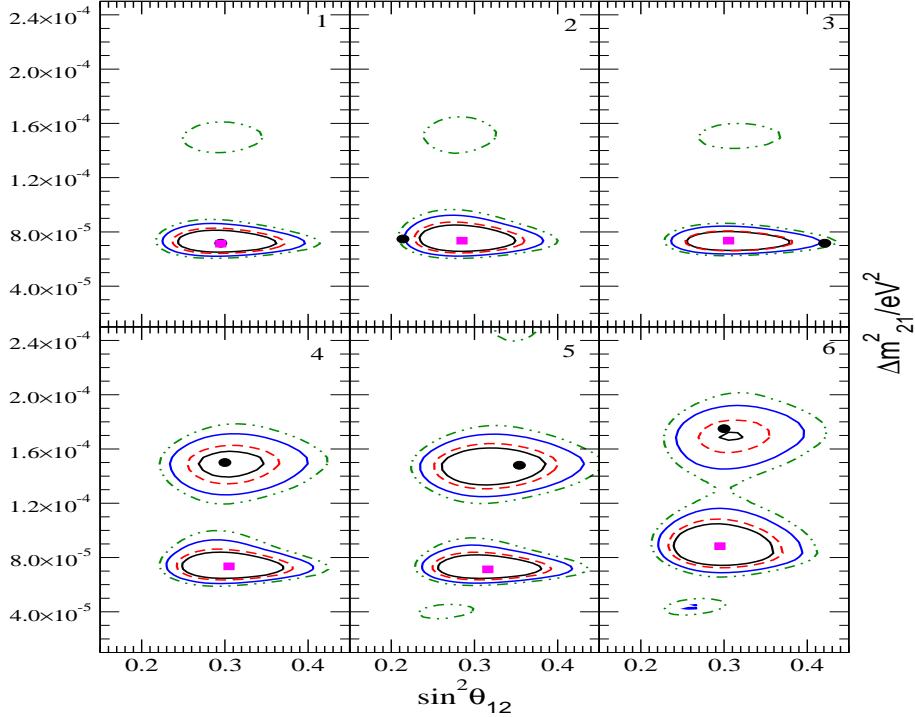


Figure 8: The 90%, 95%, 99% and 99.73% C.L. allowed regions obtained from a combined analysis using the global solar neutrino data and a 0.41 kTy simulated KamLAND data. The points in the parameter space, for which the 0.41 kTy KamLAND data has been simulated, are shown by the black dots; they have been chosen to lie within the current 3σ allowed regions. The best-fit point of the combined analysis are shown as red “boxes”.

We expect the best precision measurement results from the reactor experiment KamLAND [29, 30]. With 1 kTy statistics in KamLAND data one might expect to reduce the uncertainty in the Δm_{21}^2 determination to a few percent [13, 27]. In Figures 8 and 9 we present the two-neutrino mixing allowed regions in the solar neutrino oscillation parameter space from a combined analysis using the current global solar neutrino data and a prospective 0.41 kTy⁴ and 1.0 kTy simulated data in KamLAND. Since in future the systematic uncertainty in KamLAND is expected to be reduced (especially with the fiducial volume calibration), we use a value of 5% for the KamLAND systematic error in this analysis. The black dots in the various panels of Figures 8 and 9 denote the point in the parameter space for which the data has been simulated. The pink squares give the points where we get the best-fit for the joint analysis. For the first rows of panels,

⁴This corresponds to 2.5 times the statistics of the first published data from KamLAND.

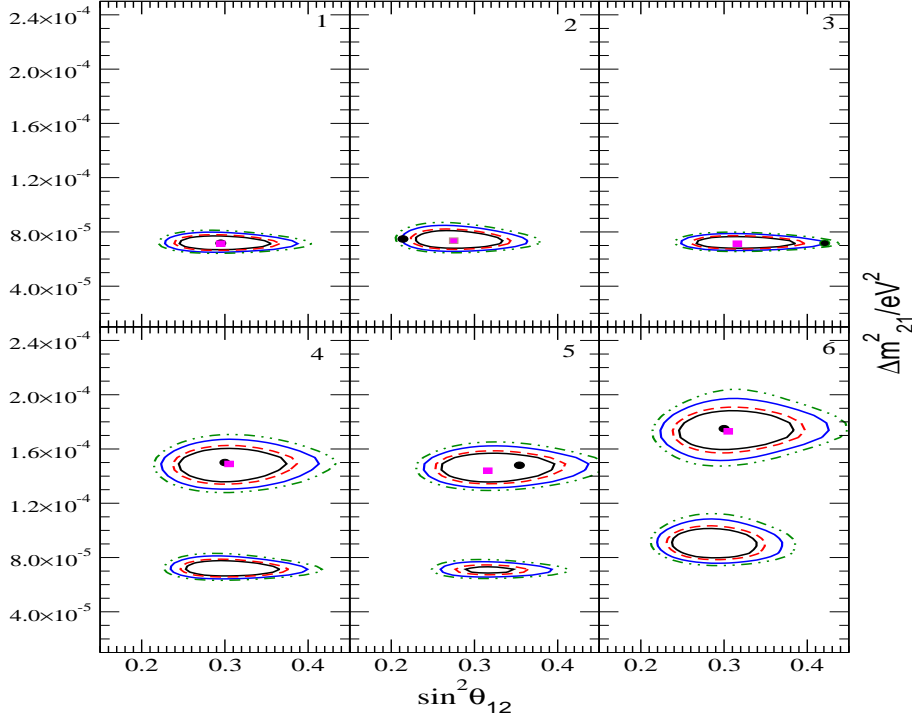


Figure 9: Same as Fig. 8, but for 1 kTy statistics.

the points at which we simulate the KamLAND data lie in the low-LMA region. We note that if the true solution lies in the low-LMA region, a spurious high-LMA solution still appears at 3σ level in the case of 0.41 kTy of statistics, though the allowed area gets further reduced in size, owing to the precision of the KamLAND data. The high-LMA solution disappears if the statistics is increased to 1.0 kTy. For all the panels the precision on the range of allowed value of Δm_{21}^2 is seen to improve. There is little improvement, however, in the precision of $\sin^2 \theta_{12}$ [27] (see also [31]). In the last rows of Figures 8 and 9 we illustrate a scenario that would show itself if the future KamLAND data conforms to a point in the high-LMA region. Since the low-LMA solution is now strongly favored over the high-LMA one by the global solar neutrino data, if such a contradictory situation arises whereby the KamLAND data alone would favor the high-LMA solution, both solutions would get allowed and the solution ambiguity would remain. As can be seen in the last row panels of Figures 8 and 9, the best-fit point comes in the low-LMA (high-LMA) region for 0.41 kTy (1 kTy) statistics. We have checked that if we simulate the spectrum in the high-LMA region, the best-fit shifts from the low-LMA to the high-LMA region after KamLAND collects about 1 kTy statistics.

6 Conclusions

We analysed the impact of the salt phase data from the SNO experiment in global solar neutrino oscillation analysis, including the KamLAND data as well. The inclusion of the CC and NC event rates from the SNO salt phase data firmly establishes Δm_{21}^2 to lie in the low-LMA region. Values of Δm_{21}^2 in the LOW area get disfavoured at more than 3σ just from global solar neutrino data, and at almost 5σ from the combined solar and KamLAND data. The combined effect of the SNO spectrum data from the D_2O phase and of the data from the salt phase results in lowering the upper bound on Δm_{21}^2 to $\Delta m_{21}^2 \leq 1.7 \times 10^{-4} \text{ eV}^2$ (99.73% C.L.). The global solar + KamLAND data still admit the high-LMA solution, but it appears only at 3σ level. The addition of the new SNO data restricts the mixing angle θ_{12} from above and maximal mixing is now excluded at more than 5σ . With the inclusion of non-zero values of the mixing angle θ_{13} in a 3-neutrino mixing analysis, the allowed regions in the $\Delta m_{21}^2 - \sin^2 \theta_{12}$ plane decrease in size as θ_{13} increases. At $\sin^2 \theta_{13} \geq 0.075$ no allowed regions are obtained at 99.73% C.L. The solution due to transitions into sterile neutrino is excluded at 7.8σ with the salt phase data. However, solar ν_e transitions into a mixed sterile + active state are allowed, with the sterile fraction restricted to be $< 52\%$ at 3σ . With the knowledge of Δm_{21}^2 and $\sin^2 \theta_{12}$ responsible for the solar neutrino oscillations becoming more precise, the predicted ranges for the day-night asymmetry in SNO, and of the event rates in Borexino and the LowNU, experiments narrow down. We also studied the impact of prospective KamLAND data statistics increase to 0.41 kTy and 1.0 kTy for the determination of the solar neutrino oscillation parameters. If the spectrum is simulated at a point in the low-LMA region, the allowed 3σ area in the high-LMA zone reduces in size in the case of 0.41 kTy of data, and disappears if the statistics is increased to 1.0 kTy. If, however, the KamLAND spectrum corresponds to a point in the high-LMA zone, the conflicting trend of solar and KamLAND data would make the high-LMA solution reappear at 90% C.L. and the determination of Δm_{21}^2 would remain ambiguous.

S.G. would like to thank The Abdus Salam International Centre for Theoretical Physics for hospitality.

References

- [1] S. N. Ahmed *et al.* [SNO Collaboration], arXiv:nucl-ex/0309004.
- [2] B. Pontecorvo, *Zh. Eksp. Teor. Fiz.* **53** (1967) 1717.
- [3] B. Pontecorvo, Chalk River Lab. report PD-205, 1946.
- [4] R. Davis, D.S. Harmer and K.C. Hoffman, *Phys. Rev. Lett.* **20**, 1205 (1968); R. Davis, Proc. of the “Neutrino ‘72” Int. Conference, Balatonfured, Hungary, June 1972 (eds. A. Frenkel and G. Marx, OMKDK-TECHNOINFORM, Budapest, 1972), p.5.
- [5] B. T. Cleveland *et al.*, *Astrophys. J.* **496**, 505 (1998); J. N. Abdurashitov *et al.* [SAGE Collaboration], arXiv:astro-ph/0204245; W. Hampel *et al.* [GALLEX Collaboration], *Phys. Lett. B* **447**, 127 (1999); E. Bellotti, Talk at Gran Sasso National Laboratories, Italy, May 17, 2002;

- T. Kirsten, talk at *Neutrino 2002*, XXth International Conference on Neutrino Physics and Astrophysics, Munich, Germany, May 25-30, 2002. (<http://neutrino2002.ph.tum.de/>)
- [6] S. Fukuda *et al.* [Super-Kamiokande Collaboration], *Phys. Lett. B* **539**, 179 (2002) [arXiv:hep-ex/0205075].
- [7] Q. R. Ahmad *et al.* [SNO Collaboration], *Phys. Rev. Lett.* **87**, 071301 (2001) [arXiv:nucl-ex/0106015].
- [8] Q. R. Ahmad *et al.* [SNO Collaboration], *Phys. Rev. Lett.* **89**, 011301 (2002) [arXiv:nucl-ex/0204008]. Q. R. Ahmad *et al.* [SNO Collaboration], *Phys. Rev. Lett.* **89**, 011302 (2002) [arXiv:nucl-ex/0204009];
- [9] L. Wolfenstein, *Phys. Rev. D* **17**, 2369 (1978) ; S. P. Mikheev and A. Y. Smirnov, *Sov. J. Nucl. Phys.* **42** (1985) 913 [*Yad. Fiz.* **42**, 1441 (1985)].
- [10] A. Bandyopadhyay, S. Choubey, S. Goswami and K. Kar, *Phys. Lett. B* **519**, 83 (2001) [arXiv:hep-ph/0106264].
- [11] A. Bandyopadhyay, S. Choubey, S. Goswami and D. P. Roy, *Phys. Lett. B* **540**, 14 (2002) [arXiv:hep-ph/0204286]. S. Choubey, A. Bandyopadhyay, S. Goswami and D. P. Roy, arXiv:hep-ph/0209222.
- [12] K. Eguchi *et al.* [KamLAND Collaboration], *Phys. Rev. Lett.* **90**, 021802 (2003) [arXiv:hep-ex/0212021].
- [13] A. Bandyopadhyay, S. Choubey, R. Gandhi, S. Goswami and D. P. Roy, *Phys. Lett. B* **559**, 121 (2003) [arXiv:hep-ph/0212146];
- [14] G. L. Fogli *et al.*, *Phys. Rev. D* **67**, 073002 (2003) [arXiv:hep-ph/0212127]; M. Maltoni, T. Schwetz and J. W. Valle, arXiv:hep-ph/0212129; J. N. Bahcall, M. C. Gonzalez-Garcia and C. Pena-Garay, *JHEP* **0302**, 009 (2003) [arXiv:hep-ph/0212147]; H. Nunokawa, W. J. Teves and R. Zukanovich Funchal, arXiv:hep-ph/0212202; P. Aliani *et al.*, arXiv:hep-ph/0212212; P. C. de Holanda and A. Y. Smirnov, *JCAP* **0302**, 001 (2003) [arXiv:hep-ph/0212270].
- [15] M. Apollonio *et al.*, *Phys. Lett.* **B466** (1999) 415; F. Boehm *et al.*, *Phys. Rev.* **D62** (2000) 072002.
- [16] S.M. Bilenky, D. Nicolo and S.T. Petcov, *Phys. Lett.* **B538** (2002) 77.
- [17] Super-Kamiokande Coll., Y. Hayato *et al.*, Talk given at the Int. EPS Conference on High Energy Physics, July 17 - 23, 2003, Aachen, Germany.
- [18] [Super-Kamiokande Collaboration], arXiv:hep-ex/0309011.
- [19] “HOWTO use the SNO Salt Flux Results”, and “HOWTO use the SNO Solar Neutrino Spectral data”, SNO Collaboration, <http://www.sno.phy.queensu.ca/>;

- [20] M. Maris and S. T. Petcov, Phys. Lett. B **534** (2002) 17 [arXiv:hep-ph/0201087], and Phys. Rev. D **62**, 093006 (2000). (arXiv:hep-ph/0003301).
- [21] S.T. Petcov, Phys. Lett. B **214**, 259 (1988).
- [22] S.T. Petcov, Phys. Lett. B **200**, 373 (1988), and Phys. Lett. B **214**, 139 (1988); S.T. Petcov and J. Rich, Phys. Lett. B **224**, 401 (1989); P.I. Krastev and S.T. Petcov, Phys. Lett. B **207**, 64 (1988); E. Lisi et al., Phys. Rev. D **63**, 093002 (2000).
- [23] C. Athanassopoulos *et al.*, (The LSND Collaboration) Phys. Rev. Lett. **77**, 3082 (1996); C. Athanassopoulos *et al.*, (The LSND Collaboration) Phys. Rev. Lett. **81**, 1774 (1998).
- [24] J. Formaggio, talk at *5th International Workshop on Neutrino Factories & Superbeams*, NuFact '03, Columbia University, New York, 5-11 June 2003; <http://www.cap.bnl.gov/nufact03>.
- [25] G. Alimonti *et al.* [Borexino Collaboration], Astropart. Phys. **16**, 205 (2002) [arXiv:hep-ex/0012030].
- [26] S. Schönert, talk at Neutrino 2002, Munich, Germany, (<http://neutrino2002.ph.tum.de>).
- [27] A. Bandyopadhyay, S. Choubey and S. Goswami, Phys. Rev. D **67**, 113011 (2003) [arXiv:hep-ph/0302243].
- [28] J. N. Bahcall and C. Pena-Garay, arXiv:hep-ph/0305159.
- [29] A. Bandyopadhyay, S. Choubey, R. Gandhi, S. Goswami and D. P. Roy, arXiv:hep-ph/0211266.
- [30] V. D. Barger, D. Marfatia and B. P. Wood, Phys. Lett. B **498**, 53 (2001) [arXiv:hep-ph/0011251]; H. Murayama and A. Pierce, Phys. Rev. D **65**, 013012 (2002) [arXiv:hep-ph/0012075]; A. de Gouvea and C. Pena-Garay, Phys. Rev. D **64**, 113011 (2001) [arXiv:hep-ph/0107186].
- [31] S. Choubey, S. T. Petcov and M. Piai, arXiv:hep-ph/0306017.